Understanding the role of the acid sites in HMF oxidation to FDCA reaction over gold catalysts: surface investigation on $Ce_xZr_{1-x}O_2$ compounds

Cristina Megías-Sayago [†,*], *Kristina Chakarova* [‡], *Anna Penkova* [†,*], *Alice Lolli* [¥], *Svetlana Ivanova* [†], *Stefania Albonetti* [¥], *Fabrizio Cavani* [¥], *José Antonio Odriozola* [†]

[†] Departamento de Química Inorgánica e Instituto de Ciencia de Materiales de Sevilla, Universidad de Sevilla-CSIC, Américo Vespucio 49, 41092, Seville, Spain

[‡] Institute of General and Inorganic Chemistry, Bulgarian Academy of Sciences, Sofia 1113, Bulgaria

[¥] Dip. di Chimica Industriale "Toso Montanari", Università di Bologna, Viale Risorgimento 4, 40136 Bologna (BO), Italy

ABSTRACT

A series of $Ce_xZr_{1-x}O_2$ supports with different Ce/Zr molar ratios were utilized for the preparation of gold catalyst used in the selective oxidation of 5-hydroxymethyl-2-furfural to 2,5-furandicarboxylic acid. The used method of gold deposition allows the preparation of homogeneous gold particles size and shape distribution, a formulation very useful for studies dedicated to reveal the support participation in the reaction. The supports are characterized by FTIR using CO as probe molecule and the sample catalytic activity is thereafter correlated to the support acid sites distribution. The possible participation of its Lewis/Bronsted acidity in the reaction mechanism is also proposed.

KEYWORDS: gold, 5-hydroxymethyl-2-furfural, oxidation, 2,5-furandicarboxylic acid, acid sites, CeZrO, CeO_2, ZrO_2

1. INTRODUCTION

The economic and environmental impact derived from the use of fossil fuels is increasingly evident in nowadays society. The continuous exploitation of the non-renewable feedstock led to its continuous depletion and increase of the oil price, urging the findings of renewable energy sources and/or materials [1–3]. Biomass has been proposed as the most promising alternative, allowing the production of fuels and chemicals from renewable raw materials such as lignocellulosic fraction [4,5]. The number of involved processes and technologies to transform the mentioned fraction into chemicals is increasing thanks to both, new catalytic technologies and synthetic routes recently discovered. An example of such a process is the efficient conversion of furfural derivatives, synthesized by means of hydrolysis and dehydration reactions from cellulose and hemicellulose [6,7]. In particular, the 5-hydroxymethylfurfural (HMF) is considered as one of the most important platform molecules derived from the lignocellulosic biomass since it can be transformed into several compounds used for fuels or chemicals synthesis [8]. The oxidation of both, aldehydic and the alcoholic functionalities of HMF leads to the formation of 2,5-furandicarboxylic acid (FDCA), a key monomer in the synthesis of new generation polymers and plastics [9,10] such as polyethylene furandicarboxylate (PEF), considered the most competitive substitute to the commonly used polyethylene terephthalate (PET) [11]. The general HMF oxidation network includes also 5-hydroxymethyl-2-furancarboxylic acid (HMFCA), 2,5-diformylfuran (DFF) and 5-formyl-2-furancarboxylic acid (FFCA) as reaction intermediates as presented in Scheme 1.

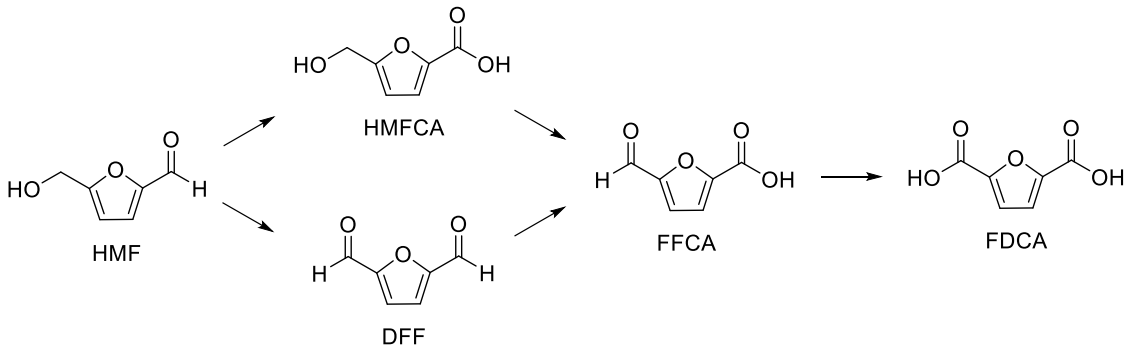

Scheme 1. General reaction network for HMF oxidation.

In the production of the FDCA, noble metal catalyzed processes result in important product yields [12–15]. Concretely, gold catalysts demonstrated relevant activity in presence of oxygen [16,17] although the use of base as co-catalyst has been established as general requirement [18,19]. This actually is considered the main drawback of the process, causing reactor corrosion or active phase leaching. For this reason, the development of highly active gold catalysts and low base concentration as co-catalyst are still serious challenges.

The supported metal nanoparticles could present different catalytic behavior depending on the used support; the interaction between gold and supports, such as CeO_2, increased the intrinsic activity of the active phase both, in gas phase oxidation reactions [20–22] and in liquid phase alcohol oxidation processes [13–15]. It is usually considered that the support Lewis acid sites are responsible for the interaction of alcohol or the forming alkoxide species as main intermediates in this process with the catalyst [23,24]. Nonetheless, there is a lack of detailed studies correlating gold catalyst activity and CeO_2 acidity and their synergy in the liquid phase selective oxidation reactions in presence of water and base.

Therefore, the aim of this work is to study the influence of the support acidity in the HMF oxidation to FDCA. For this purpose, gold was deposited over a series of

$Ce_xZr_{1-x}O_2$ supports with different Ce/Zr molar ratios. The physicochemical properties of the support and its Brönsted/Lewis acid sites interaction with CO as probe molecule were studied by FTIR spectroscopy and the results are correlated to the obtained final product yield.

2. EXPERIMENTAL SECTION

2.1. Materials

Commercially available supports CeO_2 (VP Ad Nano 90, Evonik) CeO_2(25%wt)/ZrO_2 and CeO_2(50%wt)/ZrO_2 (99%, Daiichi Kigenso Kagaku Kogio Co., Ltd) were used as received. For the preparation of the ZrO_2 support, $ZrN_2O_7{\cdot}xH_2O$ (99%, Sigma Aldrich) was used as precursor and ammonia (30%, Panreac) as precipitating agent. $HAuCl_4$ (Johnson Matthey) was used as gold precursor. For the catalytic reaction the following products were used: sodium hydroxide (≥99%, Sigma Aldrich), 5-hydroxymethylfurfural (HMF) (≥99% Ava Biochem), 2,5-furandicarboxylic acid (97% FDCA), 5-hydroxymethyl-2-furancarboxylic acid (≥99% HMFCA), 5-formyl-2-furancarboxylic acid (≥99% FFCA) and 2,5-diformylfuran (97% DFF) (the last three from Toronto Research Chemicals).

2.2 Catalyst preparation

ZrO_2 support was prepared by precipitation [25]. Zirconium precursor was dissolved upon heating and the pH was fixed to 9 by using NH_3. The obtained precipitated solid was aged for 4 h, filtered and dried at 110 ºC overnight before calcination in static air at 400 ºC for 1 h, with a heating ramp of 10 ºC/min.

Gold (2 wt% nominal value) was deposited according to the Direct Anionic Exchange (DAE) method assisted by ammonia as reported elsewhere [26]. A solution of the gold

precursor (around 10^{-4}M) was heated to 70 ºC, and then contacted with the support and 20 min later with NH_3. The final solid was filtered, dried at 100 ºC overnight and calcined at 300 ºC for 4 hours.

Ce, Ce25Zr, Ce50Zr, and Zr was the adopted nomenclature for CeO_2, CeO_2(25%wt)/ZrO_2, CeO_2(50%wt)/ZrO_2 and ZrO_2, respectively and preceded by Au for the catalysts.

2.3 Characterization

Specific surface areas of the samples were measured by N_2 physisorption equipment (Sorpty 1750 CE instruments) and the single-point BET method. All samples were previously outgassed at 150 ºC under vacuum.

XRD measurements were performed at room temperature on Panalitycal X'Pert Pro diffractometer, equipped with Cu anode. All diffractograms were recorded in the 5-90º 2θ range, with 0.05 º step size and 300 s acquisition time.

Gold contents and chemical compositions of solids were determined by X Ray Fluorescence (XRF) using Panalitycal AXIOS spectrometer with Rh tube of radiation.

FTIR spectra were recorded with a Nicolet 6700 FTIR spectrometer equipped with an MCT detector. The measurements were performed accumulating up to 64 scans at a spectral resolution of 2 cm^{-1} and accuracy of 0.01 cm^{-1}. Self-supporting wafers (≈ 10 mg cm^{-2}) or pellets pressed on W-grid were prepared from the powdered samples and treated directly in a purpose-made IR cell allowing measurements at ambient and low temperatures. The cell was connected to a vacuum-adsorption apparatus with a residual pressure lower than 10^{-3} Pa. Prior to the adsorption measurements, the samples were activated by heating in air at 300 °C and subsequent evacuation at the same temperature.

2.4 Catalytic tests

The oxidation of 5-hydroxymethylfurfural was carried out in a Parr autoclave reactor (100 mL) provided with a mechanical stirrer and temperature and pressure control. The reactor was charged with a 0.08M aqueous solution of HMF, NaOH and catalyst in a HMF:Au:NaOH molar ratio of 1:0.01:2. The metal loading experimentally obtained by XRF analysis was used to calculate the amount of catalyst according to the above mentioned ratio. Before test, the reactor was purged twice with pure O_2 and finally pressurized at 10 bars. Then the temperature was increased to 70 ºC and the reaction mixture stirred at 400 rpm for 4 hours. The reaction starts (t = 0) when the temperature reached 70 ºC (in about 10 min). After 4 hours, the reactor was cooled down to room temperature in an ice bath and the reaction mixture centrifuged and filtered. A sample was taken and diluted before analysis carried out on Agilent Infinity 1260 liquid chromatograph equipped with Aminex HPX-87H 300 mm × 7.8 mm column using 0.005 M H_2SO_4 as eluent. Conversion, selectivity and carbon balance were calculated from the peak areas, after calibration using the commercially available samples as references.

3. RESULTS AND DISCUSSION

3.1. XRD measurements

The X-ray diffraction patterns of both, supports and catalysts are shown in Fig. 1. The CeO_2 solid shows well-defined diffractions corresponding to the cubic fluorite structure (ICSD #00-034-0394). For the mixed oxides, the formation of homogeneous solid solutions and absence of segregated phases are confirmed on the basis of the diffraction patterns. In fact, all binary systems present typical diffraction patterns of $Ce_xZr_{1-x}O_2$ solid solutions [27,28]. Neither Ce50Zr nor Ce25Zr show diffractions corresponding to

pure CeO_2 and/or ZrO_2. Upon 50% Zr addition the diffractions shift to higher 2 Θ angles, attributed to ceria lattice shrinkage due to the replacement of Ce^{4+} (0.098 nm ionic radii) with smaller Zr^{4+}cations (0.084 nm) and solid solution formation. On the contrary, for the Ce25Zr solid the addition of 75% Zr suggests zirconia lattice expansion due, in this case, to the replacement of Zr^{4+}cations with bigger Ce^{4+} cations. Therefore, the Ce50Zr sample presents cubic structure (ICSD #00-028-0271), whereas Ce25Zr the tetragonal one (ICSD #01-080-0785). This is consistent with the reported literature [28]. The addition of Zr to ceria implies also a secondary effect, oxides particle size diminution, confirmed by the broadening of the diffractions for both mixed oxide samples.

For the pure ZrO_2 sample a mixture of cubic (ICSD #00-003-0640) and monoclinic (ICSD #00-007-0343) structures is observed.

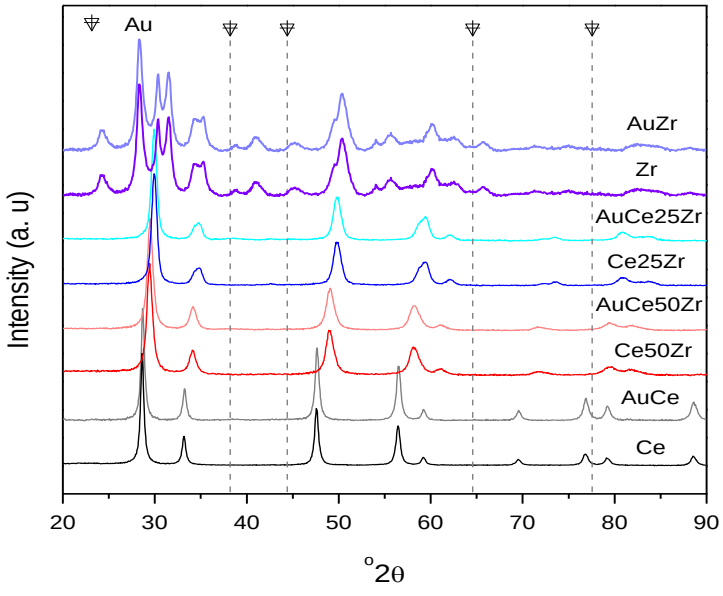

Figure 1. XRD patterns of supports and catalysts.

As for the catalysts, gold diffractions are hardly observed, suggesting particle size below 4 nm as confirmed by the TEM analysis (Table 1). As a matter of fact, the application of this method of preparation results in a very homogeneous gold particles size distribution, especially, for the catalysts supported on bare or mixed oxides with isoelectric point between 5-8, the case of all studied supports in this work [29]. The same catalysts were employed for the glucose oxidation reaction and a detailed microscopic characterization revealed that indeed the obtained gold particle size is very similar with an average value between the samples 3.6 ± 1nm [23], thus concluding that this synthetic approach is reliable and allows the preparation of small metal nanoparticles.

The actual gold loadings, particle size and textural properties of the fresh catalysts are listed in Table 1. Except for the AuCe sample, gold loadings are close to the targeted value. Both gold particle size and specific surface area are comparable for all samples. The Zr^{4+} introduction into cerium oxide lattice or vice versa does not lead to any significant change of the textural parameters.

Table 1. Characterization data of prepared catalysts.

Sample	% wt. Au	Au Particle size (nm)	Specific surface area (m^2/g)
AuCe	3.5	3.9 ± 1.5	57
AuCe50Zr	2.4	3.3 ± 1.4	55
AuCe25Zr	2.4	3.9 ± 1.2	57
AuZr	2.3	3.1 ± 1.5	70

3.2. Catalytic measurements

In general, the incorporation of Zr^{4+} to CeO_2 to form a mixed oxide leads to an increase of the metal center acidity, since the Zr-O bond is characterized by higher ionic character in comparison to the Ce-O bond [30]. For this reason, it is interesting to study in detail the influence of the support acidity in HMF oxidation reaction using as model system pure and mixed ceria-zirconia oxides (Figure 2).

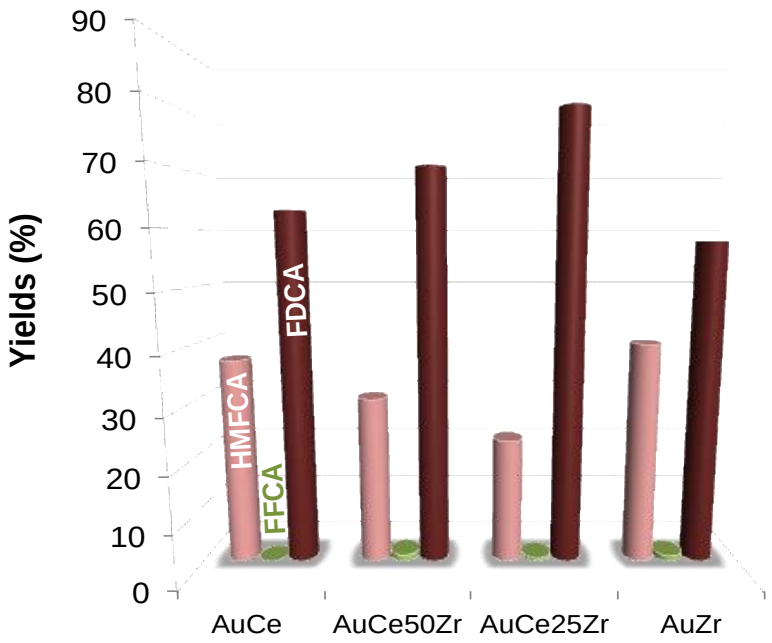

Figure 2. Products yields (%) over different gold supported catalysts in the HMF oxidation reaction. HMF conversion is complete in all cases (not plotted). Reaction conditions: HMF:NaOH:Au molar ratio 100:2:1, 10 bar O_2, 70 ºC, 400 rpm, 4h.

All studied catalysts present higher activity in comparison to previously Au-based reported systems. It is worth to mention that the catalysts are unable to convert HMF in base-free conditions making the presence of base obligatory for the reaction, as also reported in the literature[16,17,19]. The base equivalents varied a lot in all reported studies but never such a smaller quantity, like in our case, was reported (NaOH/HMF molar ratio of 2). It is very uncommon for monometallic Au supported catalyst, usually requiring higher amount of base.

The HMF conversion is complete in all cases suggesting that the activity is not influenced by the support nature but on gold presence and state. All studied catalysts are able to quickly convert HMF avoiding its degradation and by-products formation. HMFCA conversion to FFCA is reported as the rate-limiting step, but the FFCA is hardly observed due to its rapid conversion to FDCA [14,16]. The method used for gold catalyst preparation allows a very homogeneous particle size distribution, as evidenced by TEM (see SI for AuCe, AuCe25Zr, AuCe50Zr and AuZr). This fact allows us to consider similar gold surface exposed area and clearly suggests an influence of the support nature on the products yield and distribution. FDCA yield increases with the ZrO_2 content for the mixed systems but decreases in the case of bare ZrO_2. The mixed systems are the most efficient catalysts, the AuCe25Zr being the best one, leading to 80% of FDCA yield. Therefore, the general trend of activity corresponds to

AuCe25Zr (80% FDCA yield)> AuCe50Zr (70%)> AuCe (63%) > AuZr (58%).

Based on the literature data, the determining factor should be the chemical composition of the support and, particularly, its Lewis acid character and oxygen mobility. Gutiérrez-Ortiz *et al.* [28] demonstrated that the oxidation activity of C_2 chlorohydrocarbons over ceria-zirconia catalysts is a function of the Ce/Zr ratio. The incorporation of higher amounts of zirconium into ceria lattice presents a complex influence on both, acidity and reducibility/oxygen mobility of the pure parent oxide and influences the catalyst activity. On the other hand, Corma *et al.* [24] demonstrate that the gold-support collaborative effect promotes the selective oxidation of alcohols and proposes a mechanism, where both, the gold/ceria interaction and the presence of Lewis acid sites are decisive. The interaction between gold and ceria increases the population of the positively charged gold and Ce^{3+} species where the arriving alcohol interacts to give metallic alkoxide as intermediate. The latter undergoes rapid hydride transfer from

C-H to Ce^{3+} and Au^{+} to produce ketone and Ce-H, Au-H intermediates. The catalytic cycle closes after oxygen incorporation to the lattice vacancies and water release [31].

This scenario motivated us to perform a study of the acidic properties of the supports aiming to correlate them to the catalyst HMF oxidation activity. The acidity of the supports was studied by infrared spectroscopy of adsorbed CO (Figures 3-11). The adsorption experiments were preceded by activation of the samples in air for 30 min at 300°C and a consequent evacuation at the same temperature. This pretreatment was fixed to assure the physisorbed water removal without complete surface dihydroxylation mimicking the catalysts surface in aqueous reaction medium conditions. All adsorption experiments were performed at low temperature.

3.3. FTIR spectroscopy measurements

3.3.1. ZrO_2 support

The background spectrum of the activated ZrO_2 sample registered at 100 K (Fig. 3, spectrum ***a***) corresponds to a typical zirconia spectrum with two hydroxyl bands at ~ 3784 and ~ 3680 cm^{-1} (see the left inset in Fig. 3, spectrum ***a***) assigned to the ν(OH) modes of terminal and tri-bridged hydroxyl groups, respectively [32,33]. Upon addition of 5 mbar CO (Fig. 3, spectrum ***b***), carbonyl bands at 2169 (with a high frequency shoulder) and 2149 cm^{-1} evolved. The bands situated in the OH region are perturbed after CO adsorption being transformed in a wide intense band centered around 3618 cm^{-1} (Fig. 3, left inset, spectrum ***b***). During evacuation at 100 K, the 3618 cm^{-1} band gradually disappears and the original OH spectrum is restored (Fig. 3, right inset). These changes are in concert with the decrease in intensity of the carbonyl band at 2149 cm^{-1}. This allows concluding that the band positioned at 2149 cm^{-1} is due to the CO H-bonded to Zr^{4+}-OH type surface hydroxyl groups. The small shift of the 3680 cm^{-1}

band, $\Delta\nu_{(OH)} \approx$ -70 cm^{-1} (Fig. 3, left inset), indicates formation of a weak H-bond and weak acidity of the hydroxyls [34,35].

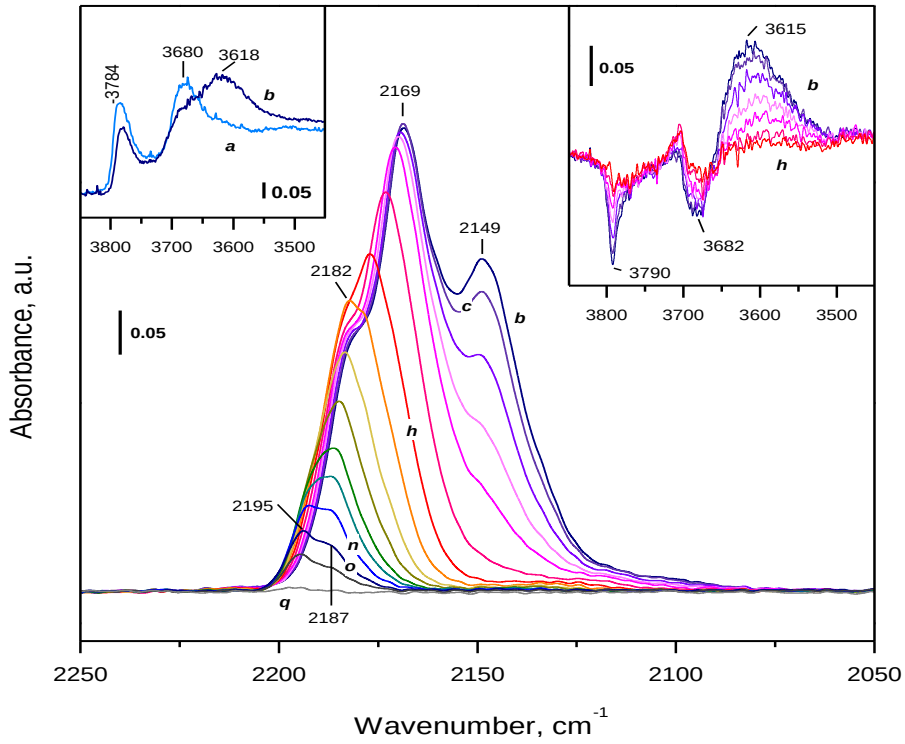

Figure 3. FTIR spectra of CO adsorbed on ZrO_2: activated sample *(a)*, in 5 mbar CO equilibrium pressure at 100 K *(b)* and during outgassing at 100 K *(c-n)* and at increasing temperatures *(o-q)*. The spectra are background and CO gas-phase corrected except for the spectra in the left inset.

The band at 2169 cm^{-1} is more stable upon evacuation suggesting that CO is adsorbed on more acidic sites, namely Zr^{4+}. This band is complex and consists of at least three components. In order to obtain deeper information about the carbonyls formed with the participation of Lewis acid sites, we have analyzed the second derivatives of the carbonyl spectra (Fig. 4). Several groups of carbonyls bands can be deduced:

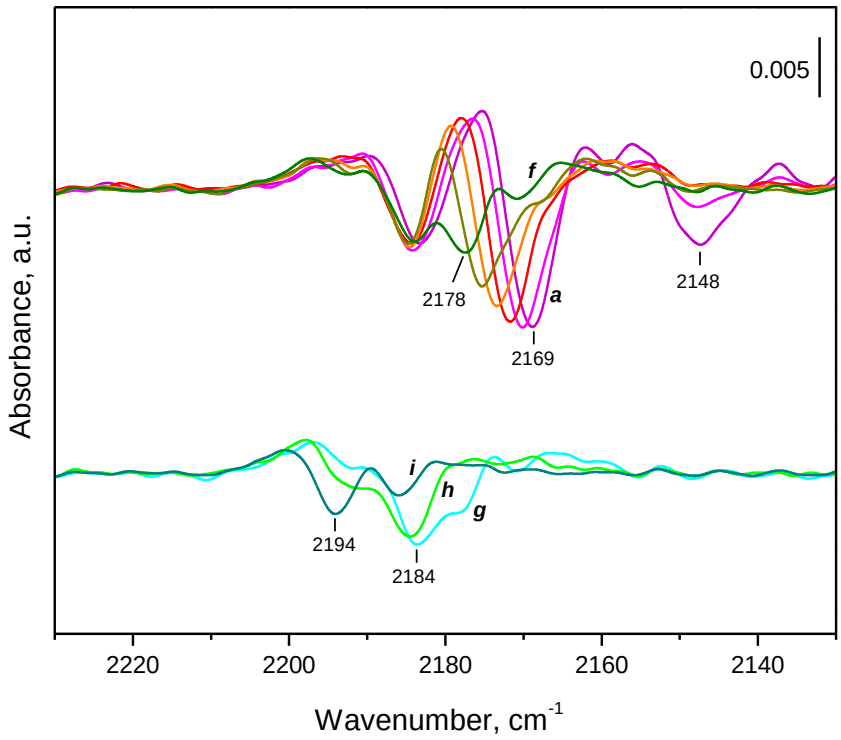

Figure 4. Second derivatives of selected spectra registered upon low-temperature adsorption of CO on ZrO_2.

i) The Zr^{4+}-OH···CO band at 2149 cm^{-1}, first disappearing during evacuation.

ii) The band at 2169 cm^{-1} gradually shifting to higher wavenumbers with CO coverage decrease. Such behavior is often observed with oxide systems, in particular with zirconia, and is known as static shift. It is due to a weakening of the cations electron-accepting properties and the occupation of the adjacent sites by the CO molecules [35,36]. Therefore, it is an indication of the presence of neighboring adsorption sites. In particular, it was related to the filling of the monoclinic *m*-ZrO_2 (111) plane [37]. This band can be then attributed to Zr^{4+}-CO species.

iii) The band at 2184 cm^{-1} not affected by the initial evacuation (Fig. 4, upper part). Prolonged evacuation causes conversion of this band into a band located at 2194

cm^{-1}. This behavior indicates that the band at 2194 cm^{-1} is due to Zr^{4+}-CO species formed with highly electrophilic and highly coordinatively unsaturated Zr^{4+} cation. At higher coverage, a second CO molecule is attached to the same zirconium site and the germinal species formed are detected at 2184 cm^{-1}. Those carbonyls are stable upon evacuation at low temperature and the bands disappear when the temperature rises.

3.3.2. CeO_2 support

After activation under the same conditions as zirconia, the low-temperature IR background spectrum of CeO_2 displays several hydroxyl bands at 3721, 3690 and 3665 cm^{-1} (Fig. 5, spectrum ***a***), suggesting presence of three different types of OHs bonded to Ce^{4+} (Ce^{4+}- OH species). In the *fluorite* type structures the oxygen atoms are tetrahedrally coordinated to Ce which may explain the existence of hydroxyl groups bonded to one, two or three metal atoms [36]. Surface hydroxyls are characterized generally by three types of sites: type I (terminal, M^{n+}−OH), type II (bridging, $(M^{n+})_2$=OH), and type III (multi-centered, $(M^{n+})_3$≡OH), the roman numbers being an indication for the coordination number of the oxygen atoms [29]. Isolated surface hydroxyls on the oxidized ceria surface manifest bands at 3710 and 3640 cm^{-1} ascribed to type I and III hydroxyls, respectively [29] and bands centered at 3655 and 3634 cm^{-1} assigned to type II hydroxyls [35]. Zaki et al. [38] also observed three bands at 3684, 3652 and 3621 cm^{-1}, assigning them to the three types of hydroxyls on Ce^{4+} sites from different fluorite structure facets. Other authors [39] have observed bands at 3690 and 3646 cm^{-1} and associated them with Ce−OH terminal hydroxyls and Ce_2(OH) doubly bridging groups interacting with the oxygen vacancies. Zaki and Knozinger [38] reported Ce^{4+}−OH bands at 3664 and 3640 cm^{-1} remaining unshifted upon CO

adsorption due to the basic character of ceria. All specified above allow us to assign the 3721 cm^{-1} band to isolated hydroxyls (type I) and the bands at 3690 and 3665 cm^{-1} to bridged hydroxyls (type II).

After addition of 5 mbar CO the OH bands moderately decreased in intensity, without changing their positions (Fig. 5, spectrum ***b***, left inset) in favor to a wide band around 3600 cm^{-1}, consequence of the formation of H-bonded hydroxyls.

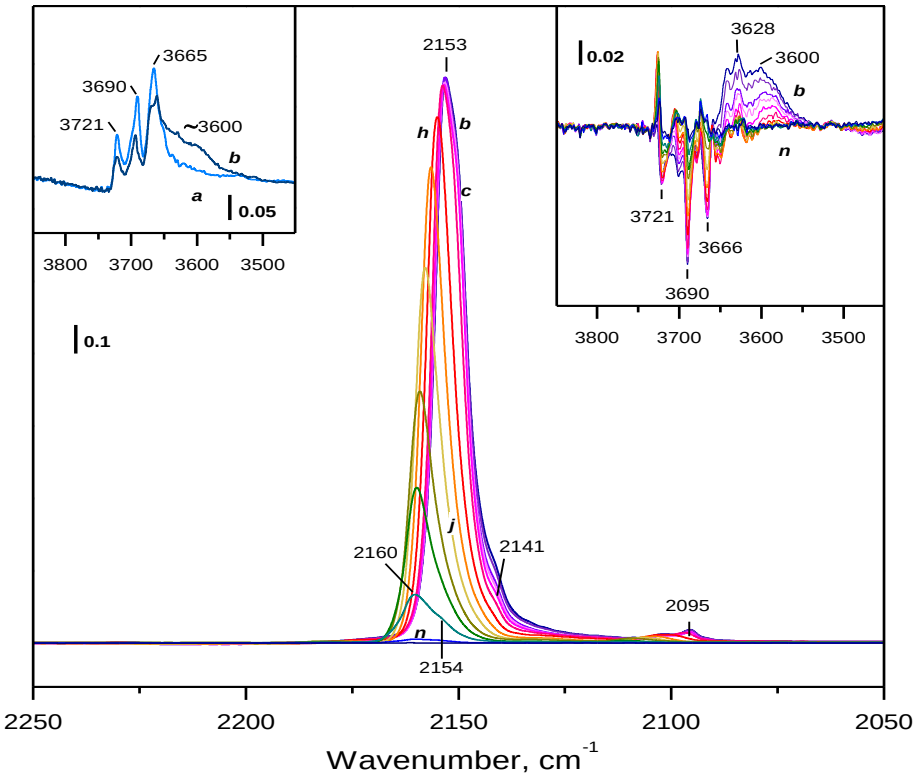

Figure 5. FTIR spectra of CO adsorbed on CeO2: activated sample (a), in 5 mbar CO equilibrium pressure CO at 100 K (b) and during outgassing at 100 K (c-n). The spectra are background and CO gas-phase corrected except for the spectra in the left inset.

Focusing in the carbonyl region after CO addition, an asymmetric band at 2153 cm^{-1} is observed, characterized by a low-frequency shoulder (2141 cm^{-1}). Since CO gas phase stretching mode is observed at 2143 cm^{-1}, the frequency of the 2141 cm^{-1} shoulder implies a very weak interaction and can be attributed to physisorbed CO. To assign properly the bands, their stability towards evacuation at low temperature (100 K) is

studied. During evacuation, the band of the physisorbed CO (2141 cm^{-1}) quickly disappears, while the band at 2153 cm^{-1} is more persistent and its maximum is gradually shifted to 2160 cm^{-1}. As the CO coverage diminishes, a new low-frequency shoulder at 2154 cm^{-1} becomes visible. Both bands disappear at low temperatures suggesting electrostatic van der Waals interaction. A similar behavior was reported by Binet et al. [34,40]. They observed an intense carbonyl band at 2151 cm^{-1} and another weak one at 2162 cm^{-1} on activated CeO_2, which disappear independently at coverage decreasing, and shift to 2157 and 2168 cm^{-1}, respectively. The high-frequency band at 2168 cm^{-1} has been attributed to carbonyls bonded to Ce^{4+} cations, and the band at 2157 cm^{-1} is assigned to a weak CO interaction with surface OH groups. Moreover, in our previous work using the same oxide [33] activated in the same conditions, a band centered at 2158 cm^{-1} is attributed to CO hydrogen bonded to Ce^{4+} hydroxyls. Careful analysis of the OH stretching region (Fig. 5, right inset), shows that at high coverage the three Ce^{4+}-hydroxyl species (isolated hydroxyls at 3721 cm^{-1} and the two different bridged hydroxyls at 3690 and 3666 cm^{-1}) decrease and transform to H-bonded hydroxyls with bands centered at 3628 and 3600 cm^{-1}. It is difficult to establish which OH group is the most affected by the CO adsorption, but one is sure, at least two H-bonded hydroxyls are observed and can be tentatively correlated to both carbonyl bands detected at 2160 and 2154 cm^{-1}. About the band at 2095 cm^{-1}, the natural abundance of ^{13}CO isotope in carbon dioxide (ca. 1%) gives rise to corresponding ^{13}CO-OH species.

Since apparently only Brönsted acid sites were detected and no indication of the Lewis sites appear, the sample was re-activated at the same temperature (300ºC) under vacuum for 15 more minutes (Fig. 6). Logically, an additional dehydroxylation occurs resulting in lower-intensity OH bands. Although, these bands are not well resolved after CO addition (Fig. 6, spectrum ***b´***), the same H-bonded hydroxyls are observed after the first

activation (Fig. 6, spectra ***b*** *and* ***b´*** and 5, spectrum ***b***). In the carbonyl region, at high coverage, in addition to the band attributed to CO hydrogen bonded to Ce^{4+}-OH, shifted to lower wavenumbers at 2150 cm^{-1} (Fig. 6, spectrum ***b´***), a band at 2167 with a shoulder at 2170 cm^{-1} (Fig. 6, spectrum ***b´*** and Fig. 7, spectrum ***b***) are observed and associated with two new Ce^{4+}-CO species. Thus a presence of two different Ce^{4+} Lewis centers are confirmed upon additional reactivation [41].

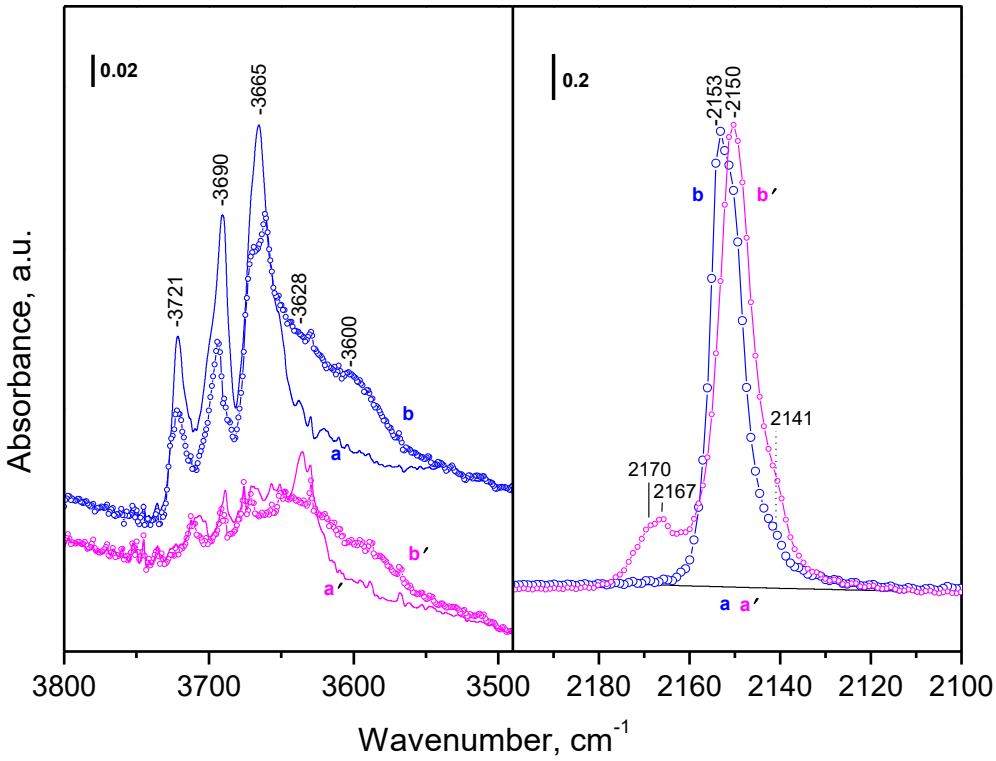

Figure 6. Blue spectra: *(a, solid line)* background spectrum of activated sample; *(b, hollow circles)* in 5 mbar CO equilibrium pressure at 100 K. Magenta spectra: *(a´, solid line)* background spectrum of activated sample subjected to additional evacuation at 300°C; *(b´ hollow circles)* in 5 mbar CO equilibrium pressure at 100 K.

When the CO coverage decreases during evacuation, a higher-frequency shift to 2175 cm^{-1} is observed (Fig. 7, left inset), attributed to the static shift and supporting the idea that both Ce^{4+}centers are not isolated. Considering the stability of all species formed

upon evacuation, both groups of carbonyls disappear at low temperature, the Ce^{4+}-CO species being more stable than the Ce^{4+}-OH···CO ones.

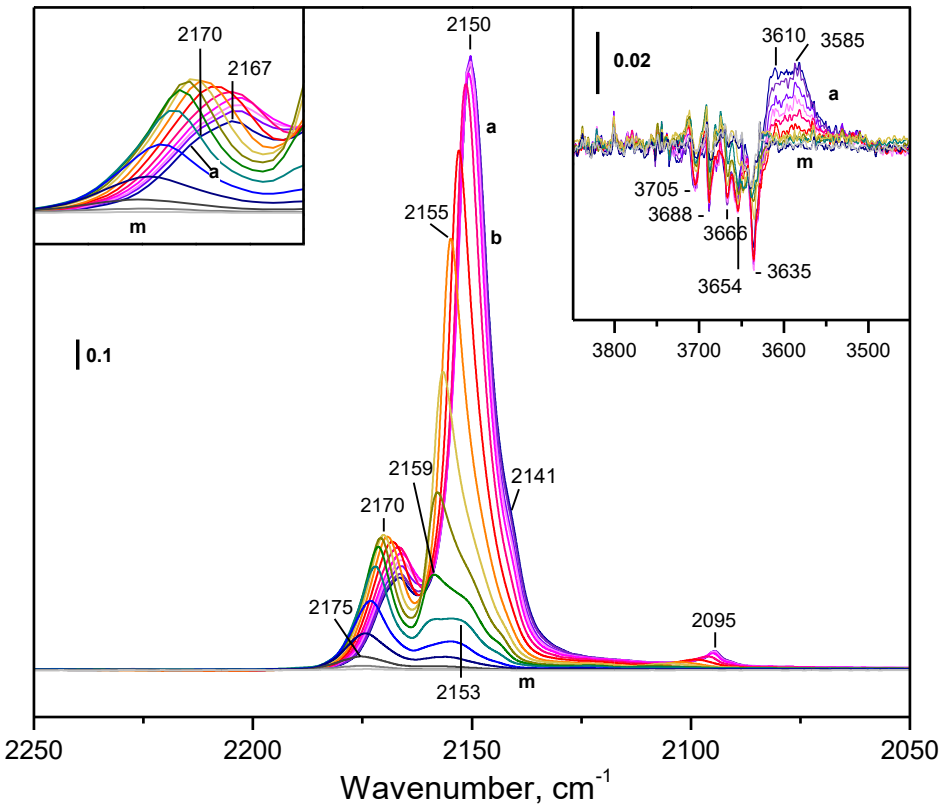

Figure 7. FTIR spectra of CO adsorbed on CeO_2: activated sample subjected to additional evacuation at 300ºC, in 5 mbar CO equilibrium pressure at 100 K (a) and during outgassing at 100 K (b-m). The spectra are background and CO gas-phase corrected.

3.3.3. Mixed CeZr supports

After activation of the mixed Ce50Zr sample several hydroxyl bands are detected, at 3782 and 3682 cm^{-1} along with another weak band at 3719 cm^{-1} (Fig. 8, spectrum ***a*** left inset). The latter is observed for ceria only and it is unambiguously assigned to Ce^{4+}-OH groups. Concerning the other two bands, they can be attributed to the pure zirconia hydroxyls, as observed above for pure ZrO_2. However, it cannot be excluded that the band at 3682 cm^{-1} could arise from hydroxyls bridging Zr and Ce cations, as a band at 3690 cm^{-1} is registered on pure ceria.

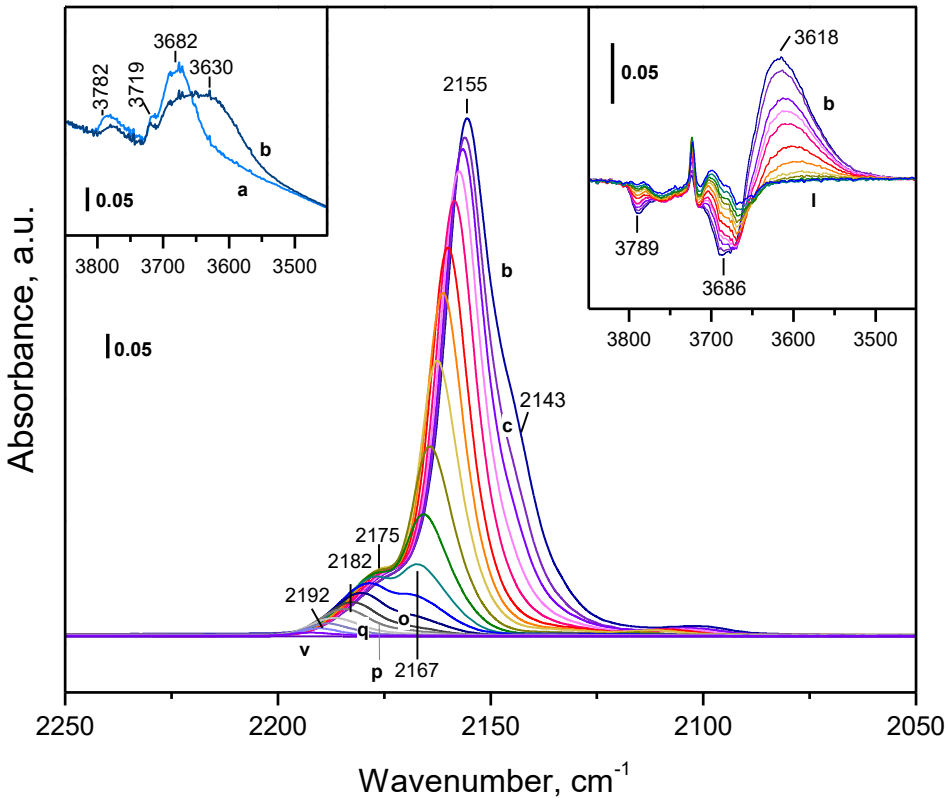

Figure 8. FTIR spectra of CO adsorbed on Ce50Zr: activated sample (a), in 5 mbar CO equilibrium pressure at 100 K (b) and during outgassing at 100 K (c-p) and at increasing temperature (q-v). The spectra are background and CO gas-phase corrected except for the spectra in the left inset.

After CO adsorption, the intensities of the hydroxyl bands diminish followed by a shift to 3618 cm^{-1} due to the formation of OH···CO species (Fig. 8, spectrum ***b***, left and right insets).

Regarding the carbonyl region, the spectrum is very similar to those of CeO_2 (see Fig. 5). An intense band at 2155 cm^{-1} slightly asymmetric around 2143 cm^{-1} and another one at 2175 cm^{-1} are registered. During the evacuation, the 2143 cm^{-1} band becomes hardly noticeable in the next spectrum, whereas the 2155 cm^{-1} band shifts to higher frequency showing a similar behaviour as the corresponding band in pure ceria. This band was attributed to Ce^{4+}-OH···CO species and the low frequency shoulder – to physisorbed CO. It should be underlined that the 2155 cm^{-1} band is less intense in

comparison to pure ceria, which suggests that the hydroxyl groups are also connected to zirconium cations. At low coverage, along with the band at 2175 cm^{-1} another band at 2167 cm^{-1} became visible. When the band at 2167 cm^{-1} is no longer evident (Fig. 8, spectrum ***o***), the only band that remains in the spectrum is centered at 2182 cm^{-1}. This band is stable at low temperature and shifts to higher frequency (2192 cm^{-1}) when the temperature increases. Taking into account that the Zr^{4+}-CO species are stable at 100 K and decomposes only with temperature increase, whereas Ce^{4+}-CO complexes decompose quickly even at low temperatures, both types of carbonyls can easily be differentiated. The bands centered at 2175 and 2167 cm^{-1} disappear at low temperature, while the band situated at 2182 cm^{-1} is more stable. Therefore, the first two bands give notice of the existence of two different Ce^{4+}sites, whereas the more stable band at 2182 cm^{-1} can be associated with Zr^{4+}-CO species, indicating higher Lewis acidity of the Zr^{4+} sites.

As for the Ce25Zr sample, the background spectrum shows the same hydroxyl bands detected for the Ce50Zr sample (Fig. 9, spectrum ***a***, left inset), the band corresponding Ce^{4+}-OH band (3719 cm^{-1}) being less intense, due to the lower ceria content.

When CO is adsorbed, the hydroxyl bands decrease in intensity and shift to lower wavenumbers (3616 cm^{-1}). In the carbonyl region, the spectra appear to be different from the Ce50Zr sample and very similar to those of pure zirconia. The bands assignment, based on the samples studied above, is as follows: 2148 cm^{-1} band corresponds to Zr^{4+}-OH···CO species; the band at 2180 cm^{-1}, stable at low temperature, is attributed to carbonyls formed with highly electrophilic and highly coordinatively unsaturated Zr^{4+} sites (converted into monocarbonyls at lower coverage); Ce^{4+} cations are detected as Ce^{4+}-OH···CO species (2159 cm^{-1}) and as Ce^{4+}-CO complexes (2171

cm^{-1}), the latter being assigned according to their lower stability as compared to zirconia carbonyls (Fig. 9, spectrum ***p***).

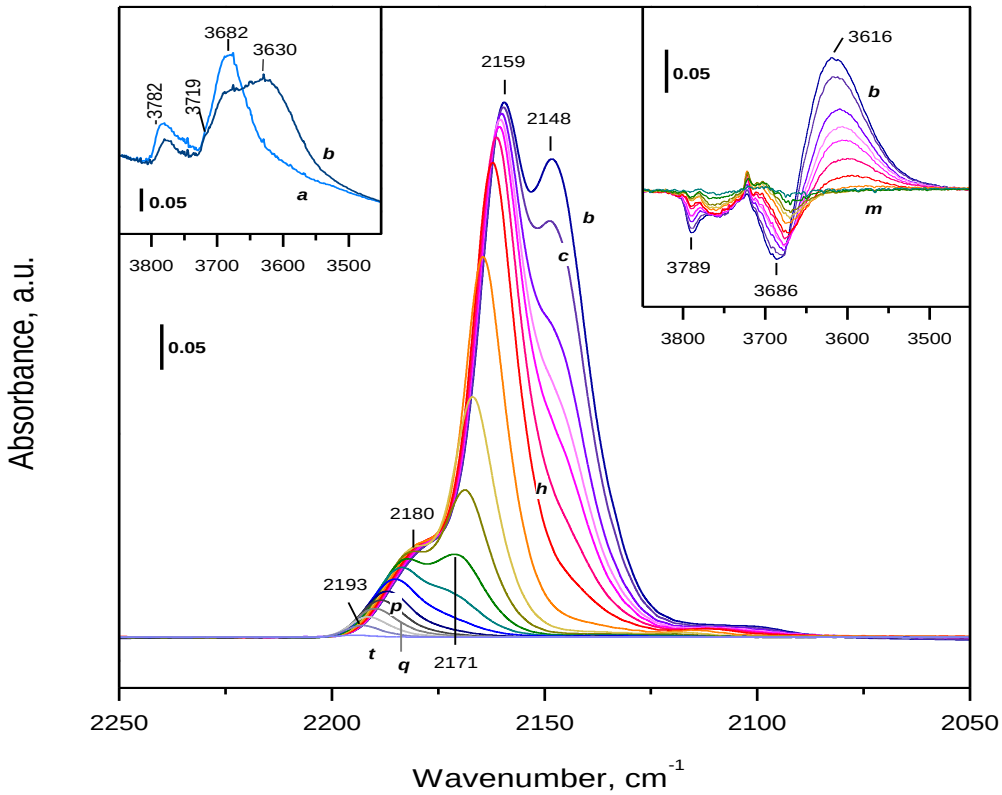

Figure 9. FTIR spectra of CO adsorbed on Ce25Zr: activated sample (a), in 5 mbar CO equilibrium pressure at 100 K (b) and during outgassing at 100 K (c-p) and at increasing temperature (q-t). The spectra are background and CO gas-phase corrected except for the spectra in the left inset.

3.3.4 Au-containing sample

In order to study the changes induced by the gold incorporation, the AuCe25Zr sample investigation followed the same methodology used with the supports (Fig. 10). In the OH region, in addition to the bands arising from the support – 3784 cm^{-1} (Zr^{4+} isolated hydroxyls) and 3676 cm^{-1} (Ce^{4+} and/or Zr^{4+} bridging hydroxyls) – a new intense band is observed at 3743 cm^{-1} (Fig. 10, spectrum ***a***, left inset). This band could be ascribed directly to gold presence, *i.e.* to Au-OH species. It is important to underline that after CO adsorption, a bigger shift of the hydroxyl bands (to 3600 cm^{-1}) is observed as

compared to the shift detected with the bare support, suggesting higher acidity of the OH species in the Au-containing sample. Regarding the carbonyl region, it is possible to observe the typical bands of Ce^{4+}-OH···CO (2161 cm^{-1}) and Ce^{4+}-CO species (observed at low CO coverage and stable at low temperature only) together with a germinal species formed on Zr^{4+} sites (2184 cm^{-1}). On the other hand, a new band centered at 2102 cm^{-1} appears and it is attributed to gold carbonyls (Au^0-CO) [42]. It should be noted that in this sample no Ce50Zr the Zr^{4+}-OH···CO species, characterized by the band at 2148 cm^{-1}, were observed. However, we do not exclude the possibility of their superimposition with the intense Ce^{4+}-OH···CO band at 2161 cm^{-1}.

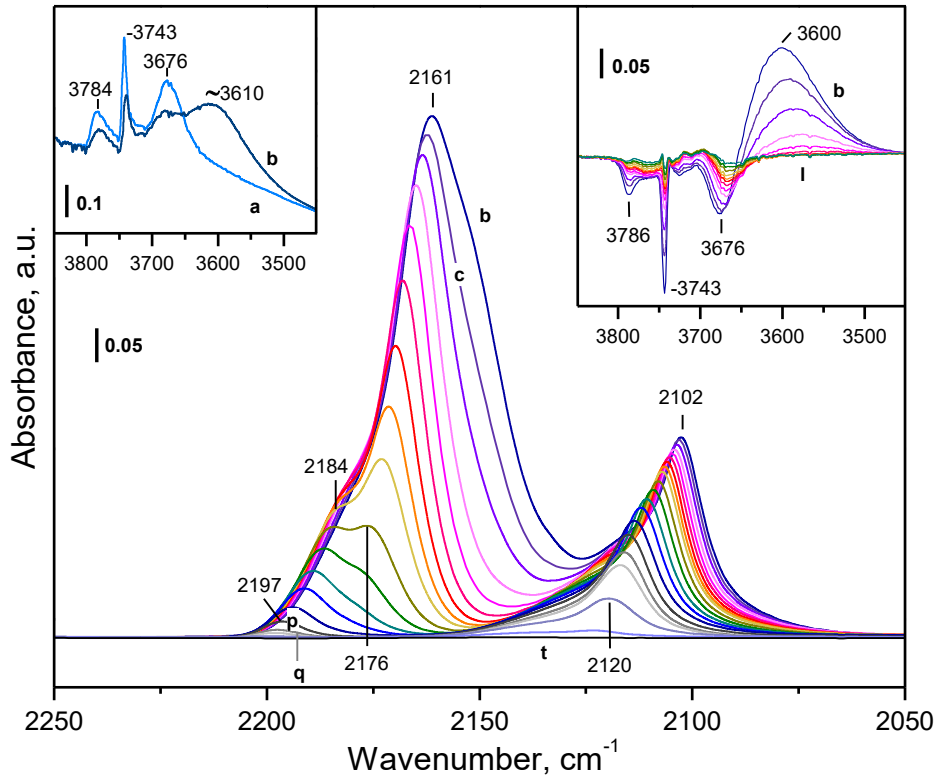

Figure 10. FTIR spectra of CO adsorbed on AuCe25Zr: activated sample (a), in 5 mbar CO equilibrium pressure at 100 K (b) and during outgassing at 100 K (c-p) and at increasing temperature (q-t). The spectra are background and CO gas-phase corrected except for the spectra in the left inset.

As a summary, Fig. 11 shows the comparison of the carbonyl region of all samples at maximal CO coverage (5 mbar equilibrium pressure).

For the pure zirconia, Zr^{4+}-OH···CO (2149 cm^{-1}) and Zr^{4+}-CO species (2169 and 2182 cm^{-1}) are detected, whereas for the ceria support only Ce^{4+}-OH···CO species (2153 cm^{-1}) are observed after the initial activation. Ce^{4+}-CO complexes (2167 and 2170 cm^{-1}) are only visible after additional activation. For the mixed Ce50Zr sample, Ce^{4+}-OH···CO species (2155 cm^{-1}), Ce^{4+}-CO complexes (2167 and 2175 cm^{-1}) and Zr^{4+}-CO carbonyls (2182 cm^{-1}) are detected. The Zr^{4+}-OH···CO species are not observed because of the presence of a significant ceria content and superimposition of the bands. When the Ce content diminish in the Ce25Zr sample, a predominant Zr^{4+} species are registered, Zr^{4+}-OH···CO (2148 cm^{-1}) and Zr^{4+}-CO (2180 cm^{-1}). The Ce^{4+} sites are detected principally as Ce^{4+}-OH···CO species (2159 cm^{-1}) and lesser amount of Ce^{4+}-CO carbonyls (2171 cm^{-1}). With the inclusion of gold to the AuCe25Zr sample, Ce^{4+}-OH···CO (2161 cm^{-1}) and Au^{0}-CO species (2102 cm^{-1}) are detected. In addition, Ce^{4+} and Zr^{4+} carbonyls (2171 and 2184 cm^{-1}, respectively) are observed. Considering the OH region, the bigger CO-induced shift of the hydroxyl band of the AuCe25Zr sample suggests a higher acidity of the corresponding hydroxyls.

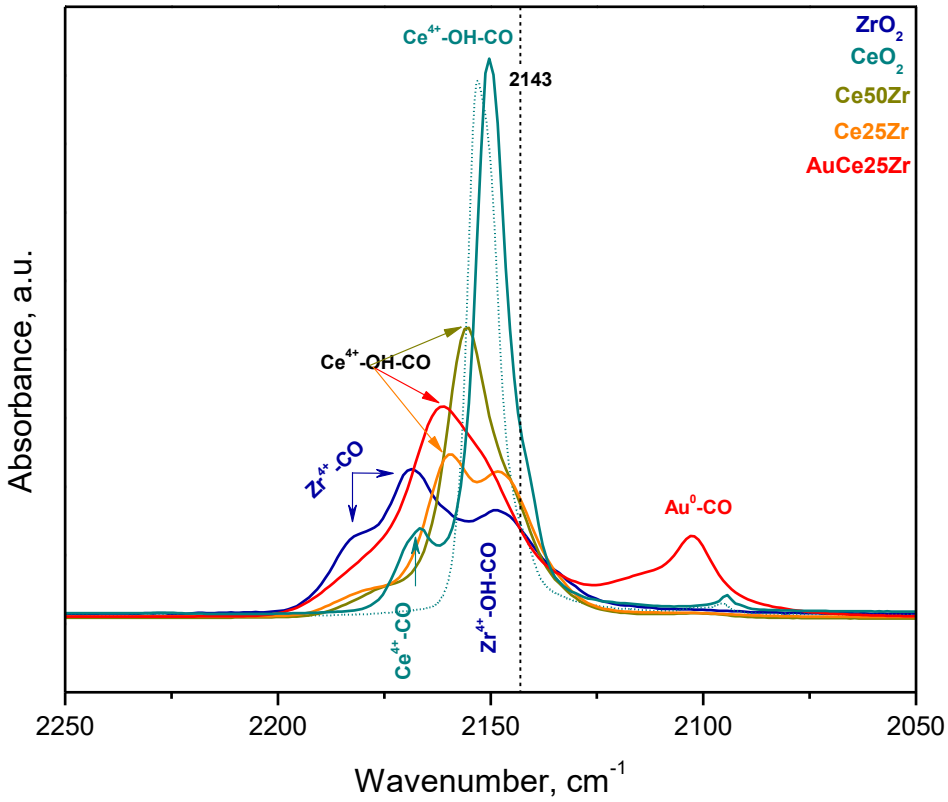

Figure 11. FTIR spectra of CO (5 mbar equilibrium pressure) adsorbed at 100 K on ZrO_2, CeO_2, Ce50Zr, Ce25Zr and AuCe25Zr. The spectra are background and CO gas-phase corrected.

Table 2 summarizes all IR bands observed in this study, where the OH bands are present on the samples before CO adsorption and all carbonyl bands appear after it.

Table 2. Summary of the IR bands observed in this study

Sample	OH bands	Bands observed after CO adsorption
ZrO_2	3784 cm^{-1} → terminal OH groups 3680 cm^{-1} → tri-bridged OH groups	2149 cm^{-1} → Zr^{4+}-OH···CO 2169 cm^{-1} → Zr^{4+}-CO 2182 cm^{-1} → $Zr^{4+}(CO)_2$ 2194 cm^{-1} → Zr^{4+}-CO formed with highly electrophilic and highly coordinatively unsaturated Zr^{4+}
CeO_2	3721 cm^{-1} → isolated (terminal) OH groups	2153 cm^{-1} → Ce^{4+}-OH···CO 2167 and 2170 cm^{-1} → two types

	3690 and 3665 cm^{-1} → bridging OH groups	Ce^{4+}-CO
Ce50Zr	3782 and 3682 cm^{-1} → Zr^{4+}-OH 3719 cm^{-1} → Ce^{4+}-OH	2155 cm^{-1} → Ce^{4+}-OH···CO 2167 and 2175 cm^{-1} → two types Ce^{4+}-CO 2182 cm^{-1} → $Zr^{4+}(CO)_2$
Ce25Zr	3782 and 3682 cm^{-1} → Zr^{4+}-OH 3719 cm^{-1} → Ce^{4+}-OH	2148 cm^{-1} → Zr^{4+}-OH···CO 2159 cm^{-1} → Ce^{4+}-OH···CO 2171 cm^{-1} → Ce^{4+}-CO 2180 cm^{-1} → $Zr^{4+}(CO)_2$
AuCe25Zr	3784 cm^{-1} → Zr^{4+}-OH 3743 cm^{-1} → Au-OH 3676 cm^{-1} → Ce^{4+} and/or Zr^{4+} bridging hydroxyls	2161 cm^{-1} → Ce^{4+}-OH···CO 2184 cm^{-1} → $Zr^{4+}(CO)_2$ 2171 cm^{-1} → Ce^{4+}-CO 2102 cm^{-1} → Au^{0}-CO

The oxidation states of the metal cations were additionally confirmed by XPS analysis (see IS).

At first sight, it is not possible to establish a clear correlation between the CO-M^{4+} bands (M = Ce, Zr) and samples catalytic activity. FDCA yield increases in the following order AuZr < AuCe < AuCe50Zr < AuCe25Zr, while the detected shift of the CO band, due to its interaction with Ce^{4+}/Zr^{4+} Lewis acid centers, follows a very different trend. The latter implies that supports Lewis acidity is not a factor controlling the catalytic performance.

On the contrary, a clear tendency is achieved considering the CO-OH-M^{4+} bands of the supports (Zr, Ce, Ce50Zr and Ce25Zr) and FDCA yield in Figure 12. Is it true that the band shift is observed for the supports but we can extrapolate this tendency to the catalysts, as the Ce/Zr ratio is the variable and the Au loading is the constant (constant HMF/Au ratio during the reaction). The FDCA yield correlates linearly with the experimentally observed M^{4+}-OH hydroxyl bands shift of supports (Table 3). Therefore, the Brönsted acidity of the OH groups is the major factor influencing the catalytic activity. It should also be underlined that, since zirconium is responsible for introducing

more hydrophilicity in the system [30], the catalyst surface will be more easily rehydroxylated, especially when water/base are present. Actually, water is responsible for Lewis acidity suppression on ZrO surface [43], since the OHs are coordinating to the acid sites, but nevertheless the increase of hydroxyl population on the surface due to the presence of Zr^{4+} cations promotes the HMF oxidation. In fact, hydroxyl ions both in reaction media and on the catalyst surface are reported to play a pivotal role in the Au-catalyzed alcohol oxidation reactions. Zope *et al.* [18] demonstrated by computational studies coupled to $^{18}O_2$ and $H_2{}^{18}O$ labeling that gold/water surfaces in presence of oxygen participate in the formation of hydroxyl ions from dioxygen and aqueous solvent, the formed ions being included in ethanol oxidation. Both, hydroxyl species and CH_3CH_2OH are adsorbed on gold before oxidation. The oxidation mechanism goes through C-H and O-H bonds activation and H extraction from alcohol molecule. Later, Davis and Zope [44] confirmed that HMF oxidation mechanism involves hydroxyl anions. The first oxidation step, the aldehyde group oxidation to form HMFCA, occurs rapidly by reaction with the solvent/base mixture. The second step, FFCA formation, involves the OH^- attack to primary alcohol carbon, being C-H and O-H bonds activated by the metal particle. The formation of dicarboxylic compound FDCA from FFCA takes place also rapidly in a similar manner as the first step. The rate-limiting step is formerly the oxidation of the alcohol group to aldehyde, *i.e.* the HMFCA oxidation [12,45,46]. For this reason, the relationship between support Brönsted acidity and catalytic activity will be focused only on this step.

Table 3. Experimentally observed M^{4+}-OH hydroxyl bands shift of supports

Sample	CO-OH-Ce^{4+}	CO-OH-Zr^{4+}
Zr	-	6
Ce	10	-
Ce50Zr	12	-
Ce25Zr	16	5

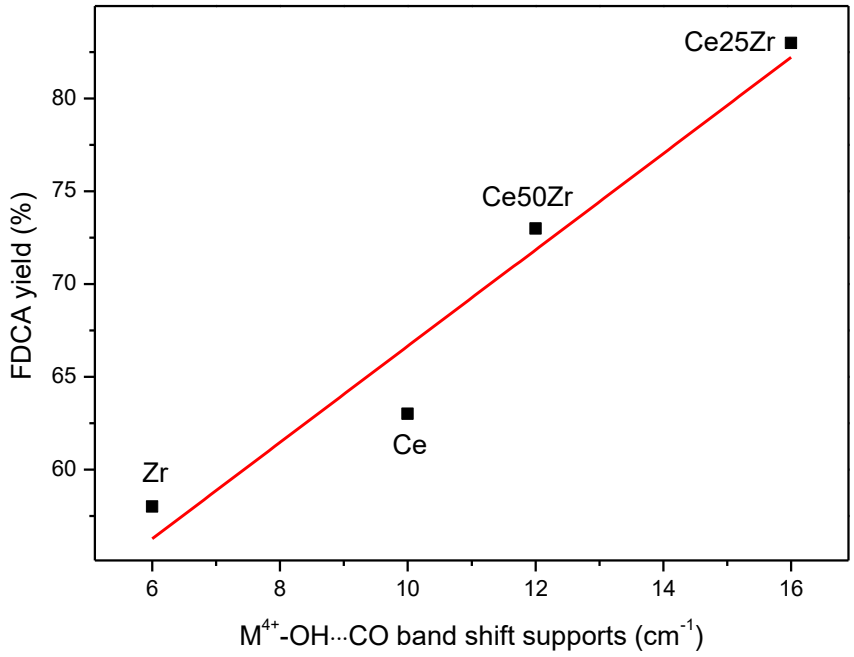

Figure 12. Correlation between FDCA yield and CO-HO-M^{4+} band shift of supports.

Higher Brönsted acidity of the support surface hydroxyl groups in aqueous basic media, in the presence of Zr^{4+} would imply a faster deprotonation leading to O^- sites density increase on the surface (Figure 13, a). The latter boosts the alkoxy intermediate formation (Figure 13, b) by means of HMFCA alcohol's deprotonation, in a similar way ethoxy formation from ethanol over homologous systems, demonstrated by Song *et al.*

[47]. Logically, as the –OH groups on the catalyst surface increases, the number of O^- surface species also increases, favoring alcohol deprotonation and alkoxy intermediate formation. The faster formation of the latter entails rapid FFCA formation and, therefore, higher FDCA yield. Simultaneously and according to the oxygen activation process proposed by Zope [18], the reactivity of the gold/water surfaces in presence of O_2 leads to OH^- formation which is the responsible for the nucleophilic attack to electrophile alkoxy carbon atom (Figure 13, b and c). Subsequently and after H abstraction, both, the water molecule and FFCA are released (Figure 13, d).

The proposed mechanism highlights the key role of Zr^{4+} in CeO_2-based systems related to the increase of the hydroxyls population and Brönsted acidity. As the proportion of Zr^{4+} increases, the number of hydroxyl groups deprotonated in basic medium also increases promoting faster formation of the alkoxy intermediate of HMFCA. This would favor FFCA formation, which is the rate-limiting step of the reaction.

In summary, two important sites are needed for the development of an efficient catalyst for sustainable FDCA production, stable non-isolated Brönsted sites situated in the vicinity of gold metal sites. The former will assure the deprotonation of the alkoxy species which will be adsorbed on gold. As much as the combination of both is present the alcohol deprotonation is favored and the subsequent nucleophile attack and H abstraction results much faster. The number of the Brönsted sites can be increased by the introduction of Zr^{4+} cations to the CeO_2-based systems.

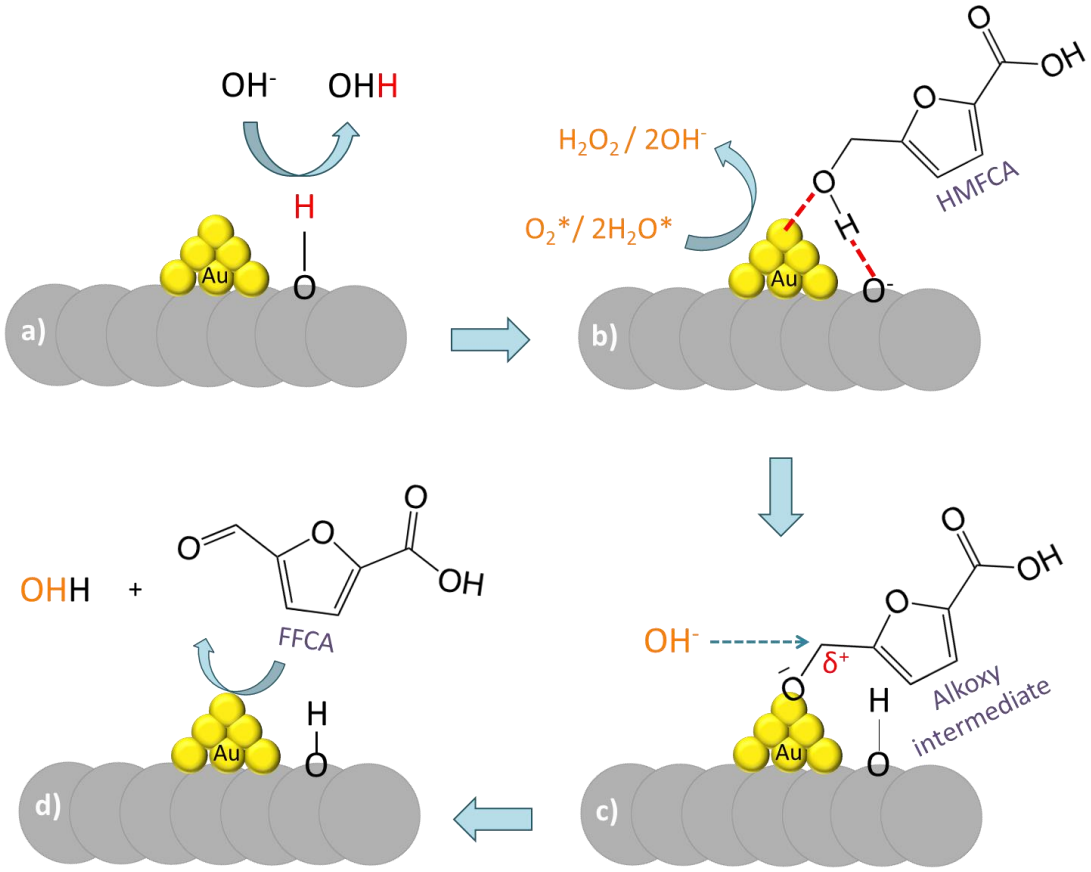

Figure 13. Proposed mechanism step: a) Deprotonation of surface hydroxyls groups in basic media, b) alkoxy intermediate formation by means of HMFCA alcohol's deprotonation over O^- sites / O_2 activation process leading to OH^- formation c) OH^- nucleophilic attack to electrophile alkoxy carbon atom and d) H_2O/FFCA formation after H^+ abstraction.

4. CONCLUSIONS

Gold was deposited on mixed or pure CeO_2, and ZrO_2 oxides, using DAE method, allowing the preparation of small size homogeneously distributed metal particles. All catalysts are very active in the HMF oxidation to FDCA with important FDCA yields at low base concentration and mild reaction conditions. The influence of the support Lewis/Brönsted acidity was studied by low temperature CO adsorption – FTIR

spectroscopy and the originated carbonyl bands corresponding to both, Lewis and Brönsted sites and their shift correlated to the catalyst selectivity. A clear trend is observed between the surface hydroxyl acidity and FDCA yield in a way that the higher the acid character, the higher the FDCA yields. It appears that the presence of Zr^{4+} increases the hydrophilicity of the support and enhances the Bronsted acidity. It should be highlighted that the support role is to facilitate the alkoxy intermediate formation potentiated by the presence of surface O^- sites (deprotonated Brönsted sites), favoring the FFCA formation and the final FDCA yield.

AUTHOR INFORMATION

Corresponding authors

*C. Megías-Sayago: cristina.megias@icmse.csic.es

*A. Penkova: apenkova@us.es

Appendix A. Supplementary data

Supplementary data associated with this article can be found, in the online version, at doi…. The file shows the TEM images and particle size distribution of the studied samples (Figure S1) and the XPS results obtained with the AuCe25Zr sample (Figures S3-S4). The XPS analysis was used for an additional verification of the obtained by IR spectroscopy oxidation states of the metal cations.

ACKNOWLEDGEMENTS

K. Chakarova acknowledges the financial support from the National Science Fund of Bulgaria (Contract No. DN 19/2). The authors acknowledge Prof. K. Hadjiivanov for contributing to a fruitful discussion.

5. REFERENCES

[1] Huber, G.W.; Chheda, J.N.; Barrett, C.J.; Dumesic, J. A. Production of Liquid Alkanes by Aqueous-Phase Processing of Biomass-Derived Carbohydrates, *Science* **2005**, 308, 1446–1450.

[2] Nigam, P.S.; Singh, A. Production of liquid biofuels from renewable resources, *Prog. Energy Combust. Sci.* **2011**, 37, 52–68.

[3] Bond, J.Q.; Alonso, D.M.; Wang, D.; West, R.M.; Dumesic, J. A. Integrated Catalytic Conversion of γ-Valerolactone to Liquid Alkenes for Transportation Fuels, *Science* **2010,** 327, 1110–1114.

[4] Corma, A.; Iborra, S.; Velty, A. Chemical routes for the transformation of biomass into chemicals, *Chem. Rev.* **2007**, 107, 2411–2502.

[5] Huber, G.W.; Iborra, S.; Corma, A. Synthesis of transportation fuels from biomass: Chemistry, catalysts, and engineering, *Chem. Rev.* **2006**, 106, 4044–4098.

[6] Climent, M.J.; Corma, A.; Iborra, S. Conversion of biomass platform molecules into fuel additives and liquid hydrocarbon fuels, *Green Chem.* **2014**, 16, 516–547.

[7] Caes, B.R.; Teixeira, R.E.; Knapp, K.G.; Raines, R.T. Biomass to Furanics : Renewable Routes to Chemicals and Fuels, *ACS Sustain. Chem. Eng.* **2015**, 3, 2591–2605.

[8] Rosatella, A.A.; Simeonov, S.P.; Frade, R.F.M.; Afonso, C.A.M. 5-Hydroxymethylfurfural (HMF) as a building block platform: Biological properties, synthesis and synthetic applications, *Green Chem.* **2011**, 13, 754–793.

[9] Werpy, T.; Peterson, G. Top Value Added Chemicals from Biomass: Volume I - Results of Screening for Potential Candidates from Sugars and Synthesis Gas. United States: N. p., **2004**. Web. doi:10.2172/15008859.

[10] Bozell, J.J.; Petersen, G.R. Cutting-edge research for a greener sustainable future Technology development for the production of biobased products from biorefinery carbohydrates — the US Department of Energy's "Top 10" revisited, Gre. **2010**, 12, 539–554.

[11] Gandini, A.; Silvestre, A.J.D.; Neto, C.P.; Sousa, A.F.; Gomes, M. The furan counterpart of poly(ethylene terephthalate): An alternative material based on renewable resources, *J. Polym. Sci. A Polym. Chem.* **2008**, 47, 295–298.

[12] Davis, S.E.; Houk, L.R.; Tamargo, E.C.; Datye, A.K.; Davis, R.J. Oxidation of 5-hydroxymethylfurfural over supported Pt , Pd and Au catalysts, *Catal. Today.* **2011**, 160, 55–60.

[13] Sahu, R.; Dhepe, P.L. Synthesis of 2,5-furandicarboxylic acid by the aerobic oxidation of 5-hydroxymethyl furfural over supported metal catalysts, *Reac. Kinet. Mech. Cat.* **2014**, 112, 173–187.

[14] Siyo, B.; Schneider, M.; Radnika, J.; Pohl, M.-M.; Langer, P.; Steinfeldt, N. Influence of support on the aerobic oxidation of HMF into FDCA over preformed Pd nanoparticle based materials, *Appl. Catal. A Gen.* **2014**, 478, 107–116.

[15] Ait Rass, H.; Essayem, N.; Besson, M. Selective Aerobic Oxidation of 5-HMF into 2 , 5- Furandicarboxylic Acid with Pt Catalysts Supported on TiO2- and ZrO2-Based supports, *ChemSusChem.* **2015**, 8, 1206–1217.

[16] Albonetti, S.; Lolli, A.; Morandi, V.; Migliori, A.; Lucarelli, C.; Cavani, F. Conversion of 5-hydroxymethylfurfural to 2 , 5-furandicarboxylic acid over Au-based catalysts : Optimization of active phase and metal – support interaction,

Appl. Catal. B, Environ. **2015**, 163, 520–530.

[17] Lolli, A.; Albonetti, S.; Utili, L.; Amadori, R.; Ospitali, F.; Lucarelli, C.; Cavani, F. Insights into the reaction mechanism for 5-hydroxymethylfurfural oxidation to FDCA on bimetallic Pd – Au nanoparticles, *Appl. Catal. A, Gen.* **2015**, 504, 408–419.

[18] Zope, B.N.; Hibbitts, D.D.; Neurock, M.; Davis, R.J. Reactivity of the Gold / Water Interface During Selective Oxidation Catalysis, *Science*. **2010**, 533, 74–79.

[19] Pasini, T.; Piccinini, M.; Blosi, M.; Bonelli, R.; Albonetti, S.; Dimitratos, N.; Lopez-Sanchez, J. A.; Sankar, M.; He, Q.; Kiely, C. J.; Hutchings, G. J.; Cavani, F. Selective oxidation of 5-hydroxymethyl-2-furfural using supported, *Green Chem.* **2011**, 13, 2091–2099.

[20] Reina, T.R.; Alvarez, A.; Ivanova, S.; Odriozola, J.A.; Centeno, M.A. Influence of Vanadium or Cobalt Oxides on the CO Oxidation Behavior of Au/MOx/CeO2–Al2O3 Systems, *ChemCatChem.* **2012**, 4, 512 – 520.

[21] Reina, T.R.; Ivanova, S.; Domínguez, M.I.; Centeno, M.A.; Odriozola, J.A. Sub-ambient CO oxidation over Au/MOx/CeO2-Al2O3 (M = Zn or Fe), *Appl. Catal. A Gen.* **2012**, 58–66, 419–420.

[22] Reina, T.R.; Ivanova, S.; Idakiev, V.; Delgado, J.J.; Ivanov, I.; Tabakova, T.; Centeno, M.A.; Odriozola, J.A. Impact of Ce–Fe synergism on the catalytic behaviour of Au/CeO2–FeOx/Al2O3 for pure H2 production, *Catal. Sci. Technol.* **2013**, 3, 779–787.

[23] Megías-Sayago, C.; Ivanova, S.; López-Cartes, C.; Centeno, M.A.; Odriozola, J.A. Gold catalysts screening in base-free aerobic oxidation of glucose to gluconic acid, *Catal. Today.* **2017**, 279, 148–154.

[24] Abad, A.; Concepción, P.; Corma, A.; García, H. A Collaborative Effect between

Gold and a Support Induces the Selective Oxidation of Alcohols, *Angew. Chem., Int. Ed.* 2005, 44, 4066–4069.

[25] Letichevsky, S.; Tellez, C.A.; De Avillez, R.R.; Isabel, M.; Silva, P.; Fraga, M.A.; Appel, L.G. Obtaining CeO 2 – ZrO 2 mixed oxides by coprecipitation : role of preparation conditions, *Appl. Catal. B Environ.* **2005**, 58, 203–210.

[26] Ivanova, S.; Petit, C.; Pitchon, V. A new preparation method for the formation of gold nanoparticles on an oxide support, *Appl. Catal. A Gen.* **2004**, 267, 191–201.

[27] Thammachart, M.; Meeyoo, V.; Risksomboon, T.; Osuwan, S. Catalytic activity of CeO2–ZrO2 mixed oxide catalysts prepared via sol–gel technique: CO oxidation, *Catal. Today.* **2001**, 68, 53–61.

[28] Gutiérrez-Ortiz, J.I.; De Rivas, B.; López-fonseca, R.; González-Velasco, J.R. Combustion of aliphatic C_2 chlorohydrocarbons over ceria – zirconia mixed oxides catalysts, *Appl. Catal. A Gen.* **2004**, 269, 147–155.

[29] Ivanova, S.; Pitchon, V.; Petit, C. Application of the direct exchange method in the preparation of gold catalysts supported on different oxide materials, *J. Mol. Catal. A Chem.* **2006**, 256, 278–283.

[30] Fornasiero, P.; Balducci, G.; Di Monte, R.; Kaspar, J.; Sergo, V.; Gubitosa, G.; Ferrero, A.; Graziani, M. Modification of the Redox Behaviour of CeO_2 Induced by Structural Doping with ZrO_2, *J. Catal.* **1996**, 164, 173–183.

[31] Pushkarev, V. V.; Kovalchuk, V.I.; D'Itri, J.L. Probing Defect Sites on the CeO_2 Surface with Dioxygen, *J. Phys. Chem. B.* **2004**, 108, 5341–5348.

[32] Tsyganenko, A.A.; Filimonov, V.N. Infrared spectra of surface hydroxyl groups and crystalline structure of oxides, *J. Mol. Struct.* **1973**, 19, 579–589.

[33] Kouva, S.; Honkala, K.; Lefferts, L.; Kanervo, J. Review: monoclinic zirconia, its surface sites and their interaction with carbon monoxide, *Catal. Sci. Technol.*

2015, 5, 3473–3490.

[34] Morterra, C.; Cerrato, G.; Di Ciero, S. IR study of the low temperature adsorption of CO on tetragonal zirconia and sulfated tetragonal zirconia, *Appl. Surf. Sci.* **1998**, 126, 107–128.

[35] Hadjiivanov, K.; Vayssilov, G. Characterization of oxide surfaces and zeolites by carbon monoxide as an IR probe molecule, *Adv. Catal.* **2002**, 47, 307–511.

[36] Penkova, A.; Laguna, O.H.; Centeno, M.A.; Odriozola, J.A. CO-Induced Morphology Changes in Zn-Modified Ceria: A FTIR Spectroscopic Study, *J. Phys. Chem. C.* **2012**, 116, 5747−5756.

[37] Cerrato, G.; Bordiga, S.; Barbera, S.; Morterra, C. A surface study of monoclinic zirconia (m-ZrO2), *Surf. Sci.* **1997**, 377–379, 50–55.

[38] Zaki, M.I.; Hasan, M.A.; Al-Sagheer, F.A.; Pasupulety, L. In situ FTIR spectra of pyridine adsorbed on SiO2–Al2O3, TiO2, ZrO2 and CeO2: general considerations for the identification of acid sites on surfaces of finely divided metal oxides, *Colloids Surf., A.* **2001**, 190, 261−274.

[39] Azambre, B.; Idriss, I.; Bueno-López, A.; García-García, A. Probing the Surface of Ceria−Zirconia Catalysts Using NOx Adsorption/Desorption: A First Step Toward the Investigation of Crystallite Heterogeneity, *J. Phys. Chem. C.* **2010**, 114, 13300−13312.

[40] Bensalem, A.; Bozon-Verduraz, F.; Delamar, M.; Bugli, G. Preparation and characterization of highly dispersed silica-supported ceria, *Appl. Catal., A.* **1995**, 121, 81−93.

[41] Romero-Sarria, F.; Penkova, A.; Martinez T., L.M.; Centeno, M.A.; Hadjiivanov, K.; Odriozola, J. A. Role of water in the CO oxidation reaction on Au/CeO2: Modification of the surface properties, *Appl. Catal. B Environ.* **2008**, 84,

119–124.

[42] Penkova, A.; Chakarova, K.; Laguna, O.H.; Hadjiivanov, K.; Romero-Saria, F.; Centeno, M.A.; Odriozola, J.A. Redox chemistry of gold in a Au/FeOx/CeO2 CO oxidation catalyst, *Catal. Commun.* **2009**, 10, 1196–1202.

[43] Bolis, V.; Morterra, C.; Volante, M.; Orio, L.; Fubini, B.; Development and suppression of surface acidity on monoclinic zirconia: a spectroscopic and calorimetric investigation, *Langmuir* **1990**, 6, 695–701.

[44] Davis, S.E.; Zope, B.N.; Davis, R.J. Green Chemistry On the mechanism of selective oxidation of 5-hydroxymethylfurfural to 2 , 5-furandicarboxylic acid over supported Pt and Au catalysts, *Green Chem.* **2012**, 14, 143–147.

[45] Casanova, O.; Iborra, S.; Corma, A.; Biomass into Chemicals : Aerobic Oxidation of 5-Hydroxy-methyl-2-furfural into 2,5-Furandicarboxylic Acid with Gold Nanoparticle Catalysts, *ChemSusChem*. **2009,** 2, 1138–1144.

[46] Donoeva, B.; Masoud, N.; De Jongh, P.E.; Carbon Support Surface Effects in the Gold-Catalyzed Oxidation of 5-Hydroxymethylfurfural, *ACS Catal.* **2017,** 7, 4581−4591.

[47] Song, H.; Bao, X.; Hadad, C.M.; Ozkan, U.S. Adsorption/Desorption Behavior of Ethanol Steam Reforming Reactants and Intermediates over Supported Cobalt Catalysts, *Catal. Letters.* **2011**, 141, 43–54.